nature communications

Article

https://doi.org/10.1038/s41467-025-61659-4

Structural basis for engagement of Western Equine Encephalitis Virus with the PCDH10 receptor

Received: 12 May 2025

Accepted: 27 June 2025

Published online: 08 July 2025

Check for updates

Shengjian Liang[1,11], Yan Yang[2,11], Yixiao Liu[1,11], Zhili Xu[3,11], Jichao Hou[1,4], Donghan Li[1], Lixin Zhao[2,5], Chuyu Hu[2,5], Xiaoke Liu[1], Zihe Rao[1,3,6,7,8,9,10] ✉, Yanyi Wang[2] ✉ & Zhiyong Lou[1] ✉

PCDH10 is a newly identified general receptor for Western equine encephalitis virus (WEEV) members, a group of encephalitic alphaviruses that cause severe diseases in humans and equids. While WEEV typically binds PCDH10 as a receptor, nonpathogenic strains have evolved to lose mammalian PCDH10 binding, retaining only avian PCDH10 affinity. Virulent strains also engage VLDLR and ApoER2 as alternative receptors. Here, we determine the structure of WEEV strain 71V1658 virus-like particles (VLPs) in complex with human PCDH10 extracellular cadherin repeats 1-2 (EC1-EC2) by cryo-electron microscopy at 2.99 Å resolution. EC1 inserts into a cleft clamped by two adjacent E2-E1 heterodimers within a single trimeric spike, whereas EC2 maintains no contact with the WEEV VLP. Mutagenesis studies elucidate the impacts of the interacting residues on PCDH10. And residue 153 of E2 is crucial for PCDH10 binding, and the $_{E2}$Q153L mutation observes in the nonpathogenic strain Imperial-181 restores its ability to bind to PCDH10. Moreover, the arginine residue at position 89 on avian PCDH10 is essential for its interaction with strain Imperial-181. These results advance our understanding of receptor recognition by alphaviruses and the shift in receptor usage, providing insights for the development of antiviral therapies.

Alphaviruses are a group of positive-sense single-stranded RNA viruses that are transmitted mainly by mosquitoes and cause infectious diseases in humans and other animals[1,2]. Infection by encephalitic alphaviruses, such as Eastern, Venezuelan, and Western equine encephalitis viruses (EEEV, VEEV, and WEEV, respectively), results in encephalitis, whereas arthritogenic alphaviruses, including Chikungunya virus (CHIKV), Ross River virus (RRV), Mayaro virus (MAYV), and O'nyong-nyong virus (ONNV), cause severe arthralgia[3,4]. WEEV is an important causative agent of viral encephalitis in humans and equids, causing conditions ranging from mild flu-like illnesses to encephalitis and even

[1]School of Basic Medical Sciences, Tsinghua University, Beijing, China. [2]Key Laboratory of Virology and Biosafety, Wuhan Institute of Virology, Chinese Academy of Sciences, Wuhan, Hubei, China. [3]Division of Life Sciences and Medicine, University of Science and Technology of China, Hefei, China. [4]School of Laboratory Medicine and Life Science, Wenzhou Medical University, Wenzhou, Zhejiang, China. [5]University of Chinese Academy of Sciences, Beijing, China. [6]School of Life Sciences, Division of Life Sciences and Medicine, University of Science and Technology of China, Hefei, Anhui, China. [7]School of Life Sciences, Tsinghua University, Beijing, China. [8]State Key Laboratory of Medicinal Chemical Biology, College of Life Sciences and College of Pharmacy, Nankai University, Tianjin, China. [9]Shanghai Institute for Advanced Immunochemical Studies and School of Life Science and Technology, ShanghaiTech University, Shanghai, China. [10]National Laboratory of Biomacromolecules, CAS Center for Excellence in Biomacromolecules, Institute of Biophysics, Chinese Academy of Sciences, Beijing, China. [11]These authors contributed equally: Shengjian Liang, Yan Yang, Yixiao Liu, Zhili Xu. ✉e-mail: raozh@mail.tsinghua.edu.cn; wangyy@wh.iov.cn; louzy@mail.tsinghua.edu.cn

death[5,6]. Human WEEV infections, in particular, potentially occur directly via aerosol transmission, causing more severe encephalitis than infection via the subcutaneous route[7,8]. WEEV is therefore classified as a biological safety level 3 (BSL-3) agent; however, no therapy is clinically available for WEEV infection[9].

Alphavirus genomes encode four nonstructural proteins (nsP1–nsP4) for viral replication and five structural proteins (capsid, E3, E2, 6 K, and E1) for virus assembly[10]. The E1 protein adopts a fusion loop and is responsible for cell fusion[11], whereas the E2 protein participates in receptor binding[12–15]. A total of 240 E2-E1 heterodimers assemble into 80 trimeric spikes to form the outer glycoprotein shell of the alphavirus $T = 4$ icosahedral virion, which packages the inner nucleocapsid shell formed by 240 capsid proteins and the genomic RNA[11,16–21]. Among the 80 trimeric E2-E1 spikes, 20 trimeric spikes (named i3 spikes) are located in the 20 icosahedral threefold positions, whereas 60 trimeric spikes (named q3 spikes) are located in the 60 quasi-threefold positions.

Receptor engagement is a determinant of alphavirus entry. The mammalian Mxra8 was identified as a receptor for arthritogenic alphaviruses but not for encephalitic alphaviruses or WEEV strains[22], whereas avian Mxra8 can be used by WEEV strains as a receptor in avian reservoirs[23]. Further studies revealed that LDLRAD3, VLDLR, and ApoER2 serve as receptors for a set of alphaviruses[24,25]. Previous research has also shown how the receptors Mxra8, LDLRAD3, and VLDLR interact with various alphavirus E2-E1 proteins[23–30]. However, many WEEV strains, particularly recently identified WEEV strains with relatively low pathogenicity, cannot utilize the reported mammalian receptors for infection[31]. Recent studies revealed that protocadherin 10 (PCDH10) is a general mammalian receptor engaged by multiple WEEV strains[31,32]. PCDH10, a δ2-protocadherin, contains six extracellular cadherin repeats (EC1-EC6) and is highly expressed in neurons. It bears no structural similarity to previously identified alphavirus receptors[3,33–35]. PCDH10 supports the entry of the WEEV group A strains California, Fleming, McMillan, Y62-33, and CU71-CPA, which can also engage VLDLR and ApoER2 as receptors[31]. The WEEV group B1 strains BFS2005 and BFS932, group B2 strains Montana-64 and 71V1658, group B3 strains 85-452NM and PV012357A, and strain CBA87, which cannot utilize VLDLR and ApoER2 as receptors, were found to engage PCDH10 as the receptor[31]. In contrast, the entry of the WEEV group B3 strains R02V003422B and Imperial-181 cannot be supported by either PCDH10, VLDLR, or ApoER2. This shift in the receptor usage patterns of WEEV strains is considered associated with the variation in their mammalian virulence during submergence. The term "submergence" refers to a phenomenon characterized by a significant decline in the frequency and scale of outbreaks that occurred during the late 20th century. This decline is marked by a substantial reduction in the mammalian virulence of contemporary WEEV strains[5,6,31,36,37].

In this work, we report the cryo-EM structure of WEEV strain 71V1658 virus-like particles (VLPs) in complex with human PCDH10 EC1-EC2 at 2.99 Å. Our analysis reveals that EC1 inserts into a cleft formed by two adjacent E2-E1 heterodimers within a single trimeric spike, while EC2 does not establish any contact with the WEEV VLP. The structural analysis identifies the receptor-binding interface as comprising E2 domains A and B, along with a β-ribbon motif, and key residues from the E1 fusion loop and domain II. In addition, we performed mutagenesis studies to further explore the interaction. These studies indicate that $_{PCDH}$Q1, $_{PCDH}$N40, and $_{PCDH}$R42 play crucial roles in WEEV infection. Furthermore, residue 153 of E2 is essential for PCDH10 binding. Notably, the $_{E2}$Q153L mutation observed in the nonpathogenic strain Imperial-181 restores its ability to bind to PCDH10. Moreover, the arginine residue at position 89 on avian PCDH10 is critical for its interaction with strain Imperial-181. This atomic-level analysis of the PCDH10-WEEV interaction provides valuable insights into alphaviral entry mechanisms, receptor usage shifts during WEEV evolution, and the development of vaccines or neutralizing antibodies.

Results

Cryo-EM structure determination

The WEEV strain 71V1658 VLPs and human PCDH10-EC1-EC2 fused with a C-terminal human antibody constant region (Fc) tag were produced in HEK293F cells (Supplementary Fig. 1). A total of 3106 or 17,711 cryo-electron micrographs of WEEV VLPs alone or in complex with PCDH10-EC1-EC2-Fc, respectively, were used for further reconstruction (Supplementary Fig. 2 and Supplementary Table 1). Single-particle reconstructions with icosahedral symmetry yielded a nominal resolution of 4.50 Å or 5.90 Å with 40,222 or 17,858 good icosahedral particles for WEEV VLPs alone or in complex with PCDH10-EC1-EC2-Fc, respectively (Fig. 1a, b and Supplementary Fig. 2). To improve the densities, symmetry extension, block-based classification, and local refinement focusing on the q3 spikes were applied to achieve a final resolution of 2.53 or 2.99 Å for WEEV VLPs alone or in complex with PCDH10-EC1-EC2-Fc, respectively (Methods; Fig. 1c, d, Supplementary Figs. 2 and 3). By using the cryo-EM densities as a guide, residues 1-96 of PCDH10-EC1 in the complex were built. The models of WEEV E1 (residues 1–439) and E2 (residues 5–419) were also built in the densities. In contrast, the residues of PCDH10-EC2 and the fused Fc tag were not visible in the densities, likely due to a lack of interaction with WEEV VLPs, leading to a flexible conformation. Given that recombinant PCDH10-EC1-EC2 alone exhibited poor stability, we fused PCDH10-EC1-EC2 with an Fc tag through a flexible linker to optimize its biochemical properties, which is a widely used strategy in alphavirus receptor studies[25,30,31,38]. The lack of density corresponding to the Fc tag indicates that the fusion of PCDH10-EC1-EC2 with the Fc tag through a flexible linker would not impact the WEEV:PCDH10-EC1-EC2 interaction in structural biology and biochemical studies.

Overall structure

In the overall density of the complex, a total of 240 receptor molecules bind to WEEV VLPs, and the densities of PCDH10-EC1 present an identical binding mode at the q3 spikes and the i3 spikes (Fig. 1a). PCDH10-EC1 inserts into a cleft clamped by two adjacent E2-E1 heterodimers in the trimeric spike, where it forms contacts with E1 and E2 in one E2-E1 heterodimer (named E2-E1) and E2′ in an adjacent heterodimer (named E1′-E2′) (Fig. 2a, b). The contact surface area of PCDH10-EC1 was calculated to be 1080 Å^2, which is a significant portion of its total accessible surface area of 6,216 Å^2, indicating a strong virus–receptor interaction. The contacting areas on PCDH10-EC1 accounting for the interactions with E1, E2, and E2′ were calculated as 235 Å^2, 377 Å^2 and 468 Å^2, respectively.

Upon binding with PCDH10-EC1, the E1 and E2 proteins of WEEV VLPs exhibit local conformational changes at the interfaces (Supplementary Fig. 4a, b). Similarly, PCDH10-EC1 also shows conformational changes in the interacting region, particularly in a loop region boundaried by a disulfide bond formed by C67-C73 (Supplementary Fig. 4c). The conformations of other portions of WEEV E1/E2 and PCDH10-EC1 were not altered. Two calcium ions were identified in the crystal structure of PCDH10-EC1 (PDB: 6VG4[33]), and the side chains of their interacting residues did not show convincing density (Supplementary Fig. 4c, d). Moreover, the calcium ions are positioned remotely from the WEEV VLP interface, suggesting that the binding is likely independent of calcium ions.

Interactions of WEEV VLPs and PCDH10-EC1

The interacting residues of PCDH10-EC1 include residues $_{PCDH}$Q1 and $_{PCDH}$H3, which interact with E1; residues $_{PCDH}$Q1, $_{PCDH}$D22, $_{PCDH}$P71, $_{PCDH}$S72, $_{PCDH}$H76 and $_{PCDH}$Q89, which interact with E2; and residues $_{PCDH}$V38, $_{PCDH}$P39, $_{PCDH}$N40, $_{PCDH}$R42, $_{PCDH}$F80, $_{PCDH}$E82, $_{PCDH}$L85 and $_{PCDH}$E86 on PCDH10-EC1, which interact with E2′ in the adjacent E1′-E2′ heterodimer (Fig. 2b, c and Supplementary Table 2). These residues are distributed in four main regions (regions 1–4) (Fig. 2c).

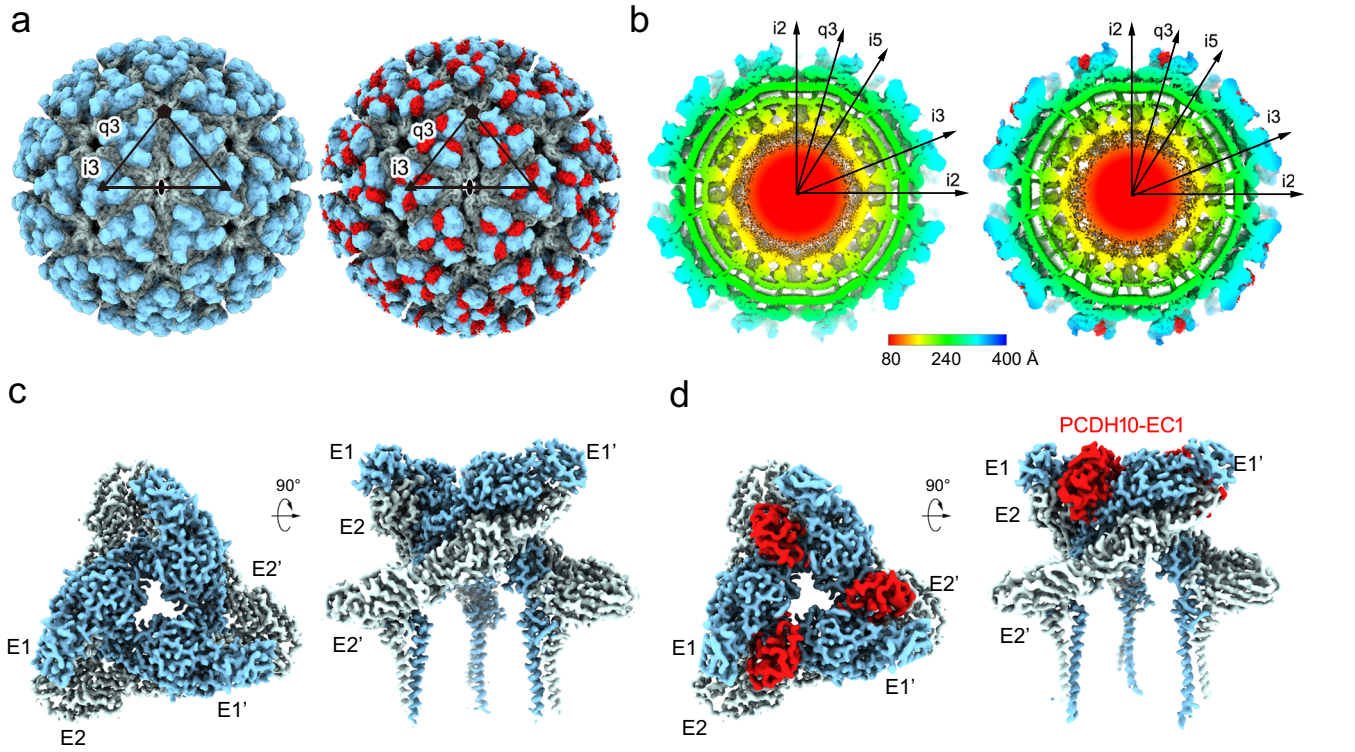

Fig. 1 | Structure of WEEV VLPs alone and in complex with PCDH10-EC1-EC2. **a** The colored surface representations of cryo-EM maps of WEEV VLPs alone (left panel) and in complex with PCDH10-EC1-EC2 (right panel). The densities of WEEV E1 and E2 proteins are colored pale cyan and light blue, whereas the densities of PCDH10-EC1 are colored red. The 5-fold, 3-fold, and 2-fold icosahedral axes are indicated by a pentagon, triangles, and an oval, respectively. The i3 spike and q3 spike are indicated by the labels "i3" and "q3" respectively. **b** The equatorial cross-sections of WEEV VLPs alone (left panel) and in complex with PCDH10-EC1-EC2 (right panel) in radial distance color scheme. The radial distances are indicated by the bar. The density of PCDH10-EC1 is separately colored red for highlighting in the right panel. **c**, **d**Cryo-EM maps achieved by the final refinement focusing on the q3 spike in WEEV VLPs alone (**c**) or in complex with PCDH10-EC1-EC2 (d). The densities are shown as a colored surface in two perpendicular views respectively.

Region 1 contains the PCDH10-EC1 residues mainly in the central β-sheet ($_{PCDH}$Q1, $_{PCDH}$H3, $_{PCDH}$D22 and $_{PCDH}$Q89), which interact with the residues of E1 ($_{E1}$F87, $_{E1}$W89 and $_{E1}$N228) and E2 ($_{E2}$F30 and $_{E2}$K181) of WEEV VLPs (Fig. 2d). In this region, the side chain of the $_{PCDH}$Q1 residue forms a hydrogen bond with the side chain of $_{E1}$N228. The side chains of residue $_{E1}$F87 in the E1 fusion loop and residue $_{E2}$F30 also offer close contact with the main-chain atoms of residue $_{PCDH}$Q1. Moreover, the large side chain of residue $_{E1}$W89 located in the E1 fusion loop stacks with the side chain of $_{PCDH}$H3. A hydrogen bond formed by the side chain of $_{PCDH}$D22 of PCDH10-EC1 and $_{E2}$K181 of E2 was also identified in this region.

In region 2, residues $_{PCDH}$P71-$_{PCDH}$S72 of PCDH10-EC1 face $_{E2}$G122 and $_{E2}$E125 of E2, forming close contacts and stabilizing the interaction of PCDH10-EC1 with WEEV VLPs (Fig. 2e). The closest intermolecular distance among the interactions in this region is ~3.2 Å, with the distances for other interactions ranging from 3.5–4.0 Å, indicating a minor role of this region in virus–receptor recognition (Supplementary Table 3).

The interaction network in region 3 consists of a loop region spanning residues $_{PCDH}$V38-$_{PCDH}$R42 of PCDH10-EC1 and residues of E2′ (including $_{E2}$D44′, $_{E2}$V158′, $_{E2}$D160′, $_{E2}$H161′, $_{E2}$L162′ and $_{E2}$T266′) (Fig. 2f). The main-chain atom of $_{PCDH}$V38 interacts with the side chain of $_{PCDH}$R42, stabilizing the conformation of $_{PCDH}$R42 together with an interaction with the side chain of $_{E2}$D160′. Residue $_{PCDH}$P39 faces $_{E2}$V158′, $_{E2}$D160′, $_{E2}$H161′, and $_{E2}$T266′, with the distances of the contacts ranging from 3.4–4.0 Å. The side chains of $_{E2}$D160′ and $_{E2}$H161′ of E2′ are close to $_{PCDH}$N40 and $_{PCDH}$R42, additionally contributing to the receptor–virus interaction.

In region 4, the side chains of $_{PCDH}$F80 and $_{PCDH}$L85 are hydrophobically packed against the side chains of $_{E2}$L153′ and $_{E2}$V269′ (Fig. 2g). Moreover, the side chain of $_{PCDH}$E82 forms a hydrogen bond with the side chain of $_{E2}$K155′. The side chain atoms of $_{E2}$L153′ are also in contact with the main-chain atoms of $_{PCDH}$L85 and $_{PCDH}$E86, playing an additional role in the interaction.

To validate whether calcium ions are required for the interaction between WEEV VLPs and PCDH10-EC1-EC2-Fc, we conducted BLI assays under calcium depletion conditions using a range of EGTA concentrations from 0 to 25.0 mM, our results showed that even at concentrations as high as 25.0 mM EGTA, the formation of the WEEV VLP:PCDH10-EC1-EC2-Fc complex was not significantly inhibited, confirming that calcium ions are not required for the interaction, consistent with the structural observations (Fig. 3a).

Mutagenesis studies of key interacting residues of PCDH10-EC1

To assess the impacts of interacting residues on virus–receptor engagement, we mutated a set of interacting residues from PCDH10-EC1-EC2-Fc and measured their binding affinities with WEEV VLPs via biolayer interferometry (BLI) (Fig. 3a). As a positive control, the wild-type (WT) PCDH10-EC1-EC2-Fc binds to WEEV VLPs with an affinity constant (K_D) of 0.234 nM. The K_D values reflect the macroscopic binding affinities between PCDH10-EC1-EC2-Fc and WEEV VLPs, whereas K_{on} and K_{off} represent the association rate constants and dissociation rate constants, respectively. The KD values obtained from BLI act as relative indicators of binding strength and show trends in affinity variations between different proteins and WEEV VLPs. However, they only offer a rough estimate of the true KD values.

https://doi.org/10.1038/s41467-025-61659-4

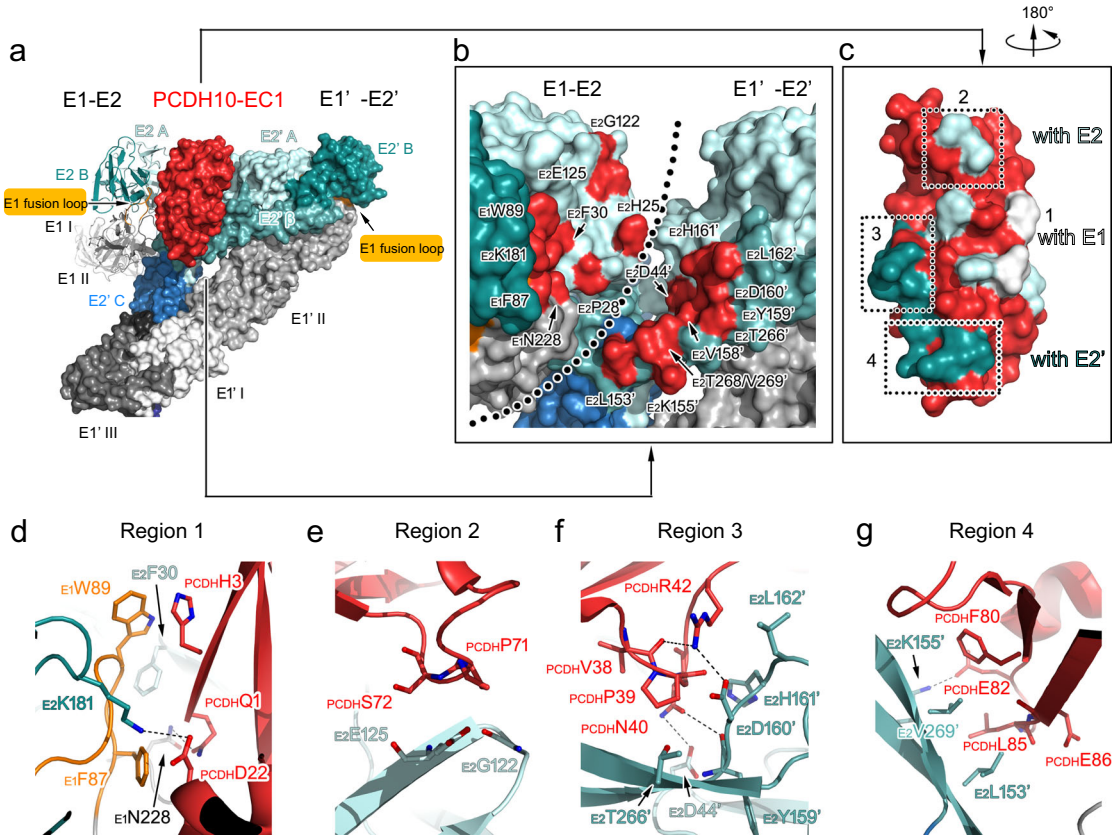

Fig. 2 | Interaction of WEEV VLP with PCDH10-EC1. a–**c** Structures of two WEEV E2-E1 heterodimers in complex with a PCDH10-EC1. **a**One E2-E1 heterodimer is shown as a colored cartoon, while the adjacent heterodimer (E1′-E2′) is covered by a molecular surface. The color scheme for E1/E2 domains and PCDH10-EC1 is as following: E1_I, white; E1_II, light gray; E1 fusion loop, orange; E1_III, gray; E1_ecto and E1_TM, deep gray; E2_A, pale cyan; E2_β, light teal; E2_B, deep teal; E2_C, sky blue; E2_TM, deep blue; PCDH10-EC1, red. **b** The E1/E2 residues that interact with PCDH10-EC1 are colored in red on the molecular surface with labels in an enlarged view. Two E2-E1 heterodimers are both covered by molecular surfaces. The boundary of two E2-E1 heterodimers is roughly indicated by a dotted line. **c** PCDH10-EC1 is covered by a molecular surface with its interacting residues for contact with E1, E2, and E2′ in white, pale cyan, and light teal, respectively. The interaction regions 2-4 are indicated by dashed frames. **d**–**g** Details for the virus-receptor interaction. The interacting regions 1 (**d**), 2 (**e**), 3 (**f**), and 4 (**g**) are presented in enlarged views. All polypeptides are shown as cartoon diagrams. Interacting residues are displayed as colored sticks with labels. The subscripts of the labels indicate the proteins that the residues belong to. Dashed lines denote the hydrogen bonds or salt bridges. For note, some interactions are not involved in these panels due to clear views and representations.

Among all the selected interacting residues, $_{PCDH}$Q1, $_{PCDH}$N40, and $_{PCDH}$R42 form strong bonds with WEEV residues in regions 1 and 3. Substitution of these residues with alanine residues eliminates the ability to bind with WEEV VLPs, which is consistent with their robust interactions with WEEV VLPs observed in the structure. To study the importance of $_{PCDH}$Q1, $_{PCDH}$N40, and $_{PCDH}$R42 for WEEV infection, HEK293T cells stably expressing the indicated PCDH10 proteins were infected with SINV-WEEV (71-V1658) (MOI = 0.5) for 9 h, and the expression of the indicated proteins was confirmed by immunoblotting (Fig. 4c). The $_{PCDH}$N40 substitution abolished the entry of SINV-WEEV, as did the $_{PCDH}$R42 substitution (Fig. 4a, b). In addition, single-residue mutation of $_{PCDH}$Q1 substantially attenuated the entry of the SINV-WEEV viruses (Fig. 4a, b). All these results acquired from cell-based assays are consistent with the binding affinities measured by BLI, indicating the key roles of $_{PCDH}$Q1, $_{PCDH}$N40, and $_{PCDH}$R42 in WEEV infection.

The $_{PCDH}$H3 residue is packed against $_{E1}$W89 at a distance of ~3.6 Å, and the side chain of $_{PCDH}$D22 forms a salt bridge with $_{E2}$K181 at a distance of ~3.2 Å. The mutations of either of these residues (PCDH10-H3A and PCDH10-D22A) result in modestly decreased binding with WEEV VLPs, with K_D values of 0.311 nM and 0.338 nM, respectively (Fig. 3a). The side chain of $_{PCHD}$H76 is packed against the side chain of $_{E2}$H25 at a distance of approximately 3.2 Å, and the disruption of this interaction by the PCDH10-H76A mutant decreased the K_D (0.507 nM) compared with that of WT PCHD10-EC1-EC2. Residue $_{PCDH}$L85 participates in hydrophobic interactions with $_{E2}$L153′, and mutation of this residue (PCDH10-L85A) resulted in a modestly attenuated K_D value of 0.330 nM. Notably, the dissociation rates for the interaction between WEEV VLPs and the PCDH10-H3A, PCDH10-D22A, PCDH10-H76A, and PCDH10-L85A mutants increased 1.9–3.2-fold, indicating that these complexes are more unstable. The PCDH10-E82A mutant presented a comparable K_D value (0.239 nM) with WT PCDH10-EC1-EC2-Fc, suggesting that the hydrogen bond (~3.0 Å) formed by the side chains of $_{PCDH}$E82 and $_{E2}$K155′ plays a minor role in virus-receptor binding.

Discussion

Strain-specific residues on the WEEV:PCHD10 interface

Since WEEV was first isolated, the scale and frequency of WEEV outbreaks and its virulence in mammals have declined, which is considered associated with a shift in receptor usage patterns during submergence[5,6,31,36,37]. The highly virulent ancestral WEEV strains engage both human PCDH10 and VLDLR/ApoER2, whereas most WEEV strains with decreased mammalian virulence are not capable of binding VLDLR/ApoER2 but retain the ability to engage human PCDH10[31]. Although PCDH10 is a general receptor for multiple WEEV strains ranging from highly pathogenic ancestral strains to newly identified nonpathogenic strains, the group B3 strains R02V003422B and

https://doi.org/10.1038/s41467-025-61659-4

a

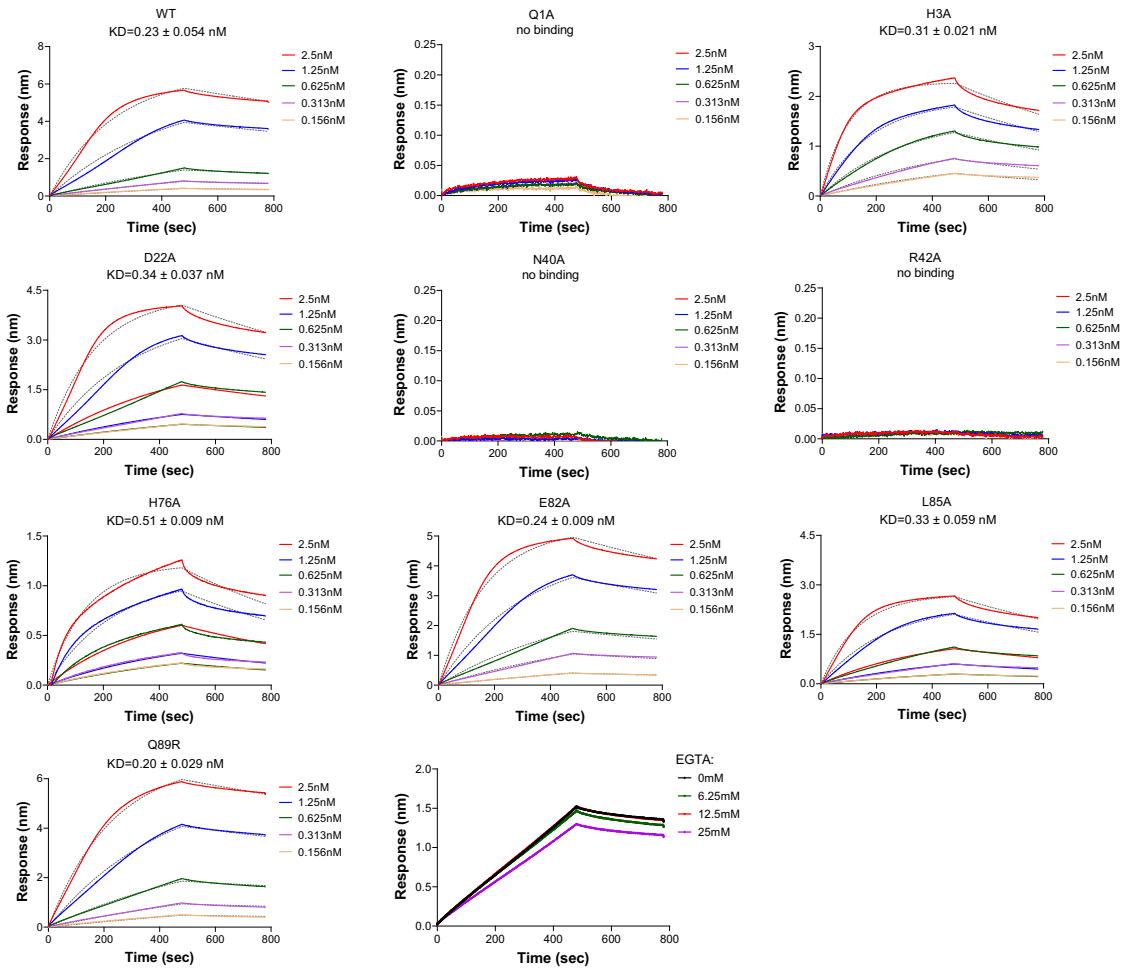

b

PCDH10-EC1-EC2	K_D (nM)		k_{on} (10^5/Ms)		k_{dis} (10^{-5}/s)	
WT	0.272 0.196	0.234	15.9 18.5	17.2	43.2 36.1	39.7
Q1A	ND ND	ND	ND ND	ND	ND ND	ND
H3A	0.326 0.296	0.311	32.7 36.3	34.5	106.5 107.5	107.0
D22A	0.364 0.311	0.338	20.8 24.4	22.6	75.6 76.0	75.8
N40A	ND ND	ND	ND ND	ND	ND ND	ND
R42A	ND ND	ND	ND ND	ND	ND ND	ND
H76A	0.513 0.500	0.507	25.8 24.5	25.2	133.0 123.0	128.0
E82A	0.245 0.233	0.239	20.5 22.3	21.4	50.4 51.9	51.1
L85A	0.372 0.288	0.330	26.5 31.5	29.0	98.7 90.7	94.7
Q89R	0.219 0.178	0.199	16.1 17.7	16.9	35.1 31.4	33.3

Fig. 3 | Binding affinities of PCDH10-EC1-EC2 or its mutants with WEEV VLPs. **a** The binding and disassociation curves of WT PCDH10-EC1-EC2 and a representative mutant PCDH10-Q1A, -D22A, -N40A, -R42A, -H76A, -E82A, -L85A, and -Q89R with WEEV 71V1658 VLPs and WT PCDH10-EC1-EC2 with WEEV 71V1658 VLPs with 0, 6.25, 12.5, 25.0 mM EGTA are shown. The calculated K_D values are displayed in each corresponding panel. The displayed results were obtained from a single technical replicate and are representative of two biologically independent experiments. The equilibrium dissociation constant (KD) was calculated as the mean ($n = 2$). **b** Summary of the measured binding affinities. The K_D value for each sample is the mean value of two independent measurements. k_{on}, association rate constant; k_{dis}, dissociation rate constant; ND, too weak interaction cannot be detected.

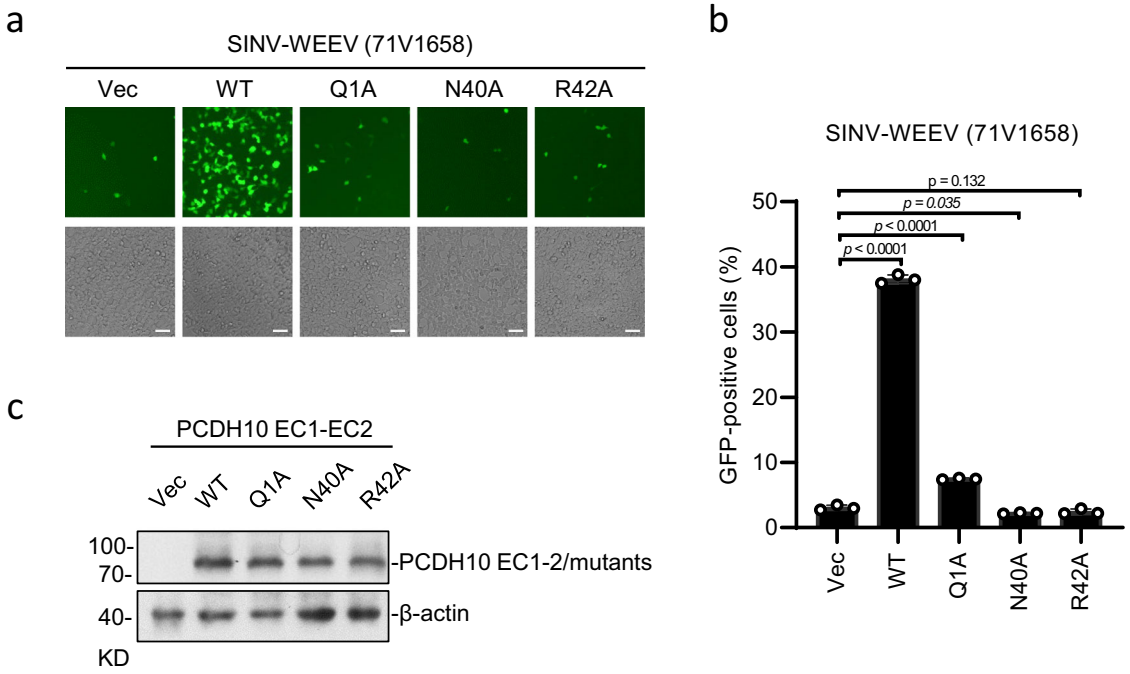

Fig. 4 | Cell-based assays for the impacts of PCDH10 mutants on WEEV infection. HEK293T cells stably expressing indicated PCDH10 proteins were infected with SINV-WEEV (71V1658) (MOI = 0.5) for 9 h. Infection was monitored by fluorescence microscopy (**a**) or flow cytometry (**b**). Expression of the indicated proteins was confirmed by immunoblots (**c**). Scale bars, 50 μm (**a**). Data are mean ± SD from 3 biological repeats, and *p*-values are from an unpaired two-tailed Student's *t* test (**b**). At least three independent experiments were performed with similar results, and representative images are shown (**a**, **c**). Source data are available as a Source Data file.

Imperial 181 cannot utilize human PCDH10 as the receptor[31]. Sequence alignment suggested that the residues that interact with WEEV E1/E2 for PCDH10 recognition are highly conserved among WEEV strains, but an exception located on the E2 protein, specifically in strains R02V003422B and Imperial 181, attracted our attention (Fig. 5a and Supplementary Figs. 5 and 6). A unique Leu-to-Gln mutation was present at position 153 of the E2 protein in strains R02V003422B and Imperial 181 compared with other strains. In the complex structure, the side chain of $_{E2}$L153 is packed against the side chains of $_{PCDH}$L85/$_{PCDH}$L87 to form hydrophobic interactions (Fig. 5a). The binding of the PCDH10-L85A mutant to WEEV VLPs is attenuated (Fig. 3a, b), suggesting that the hydrophobic interactions in this region play a role in virus-receptor engagement. Through BLI measurements, we demonstrated that PCDH10 cannot bind to WEEV strain Imperial-181 VLPs; however, the Q153L mutation in the E2 glycoprotein of WEEV strain Imperial-181 VLPs restored its ability to engage with PCDH10 (Fig. 5c). We prefer the idea that the substitution of $_{E2}$L153 with a Gln residue may disrupt the strong hydrophobic interactions in this region, which could explain the loss of binding with PCDH10 of the WEEV strains R02V003422B and Imperial 181 (Fig. 3a, b).

Notably, the WEEV strain Imperial 181 has lost the ability to bind human PCDH10, VLDLR, and ApoER2 but retains the capacity to engage avian PCDH10, indicating receptor adaptation within the enzootic cycle[31]. Among all the PCDH10 residues that interact with WEEV, position 89 is uniquely a Gln residue in human PCDH10 but is an Arg residue in mouse, horse, and sparrow PCDH10 (Fig. 5b and Supplementary Fig. 7). PCDH10-EC1-EC2-Fc with a Q89R mutation presented a slightly increased (but comparable) binding affinity (K_D = 0.199 nM) and a modestly lower dissociation rate (k_{off} = 33.3 10^{-5}/s) with WEEV than did WT PCDH10-EC1-EC2-Fc (K_D = 0.234 nM, k_{off} = 39.7 10^{-5}/s) (Fig. 3a, b). These changes may help the WEEV strain Imperial 181 retain the engagement of the PCDH10 receptor in avian reservoirs. Our further BLI measurements revealed that avian PCDH10-EC1-EC2-Fc bound to WEEV strain Imperial-181 VLPs (Fig. 5d). However, the R89Q mutation in avian PCDH10-EC1-EC2-Fc abolishes its ability to engage with WEEV strain Imperial-181 VLPs (Fig. 5d). These results validate our hypothesis that the arginine residue at position 89 on avian PCDH10 is essential for its interaction with the WEEV strain Imperial-181.

Similar to receptor usage shifts in WEEV strains, other viruses also exhibit strain-dependent changes in receptor binding. For example, DPP4 is the canonical receptor for Merbecoviruses, but recent studies identified several MERS - related coronaviruses that can use ACE2 for cellular entry[39–41]. These findings reveal molecular determinants of receptor species tropism and show that a single amino acid mutation can enable HKU5 to use human ACE2. This supports the idea that viral strains can evolve to bind alternative receptors, changing their host range and pathogenicity. Similar receptor shifts have been observed in other viral families like influenza viruses[42], where mutations in hemagglutinin or envelope proteins alter receptor binding specificities. These examples highlight the dynamic nature of virus - receptor interactions and their role in viral adaptation and emergence.

Comparison of receptor interactions of encephalitic alphaviruses

The interface of WEEV with PCDH10 differs from those observed in other encephalitic alphavirus-receptor complexes (WEEV:duMxra8(PDB: 8DAN[23]), VEEV:LDLRAD3-D1(PDB: 7N1H[29]), and EEEV:VLDLR-LA1-LA2 (PDB: 8UFC[30])) but presents several conserved regions, including residues 85-97 of WEEV E1, residues 153-166, and 180-187 of WEEV E2, as well as their counterparts in VEEV/EEEV (Fig. 5e and Supplementary Figs. 8 and 9). A notable conserved region spanning residues 153-166 of E2, or its counterparts in different viruses, was shown to participate in receptor binding in all four alphavirus–receptor complexes in our analysis, suggesting its essential role in receptor engagement of alphaviruses. Several regions are conserved in W/V/EEEV in complex with mammalian receptors. For example, the residues in the E1 fusion loop participate in receptor engagement in the

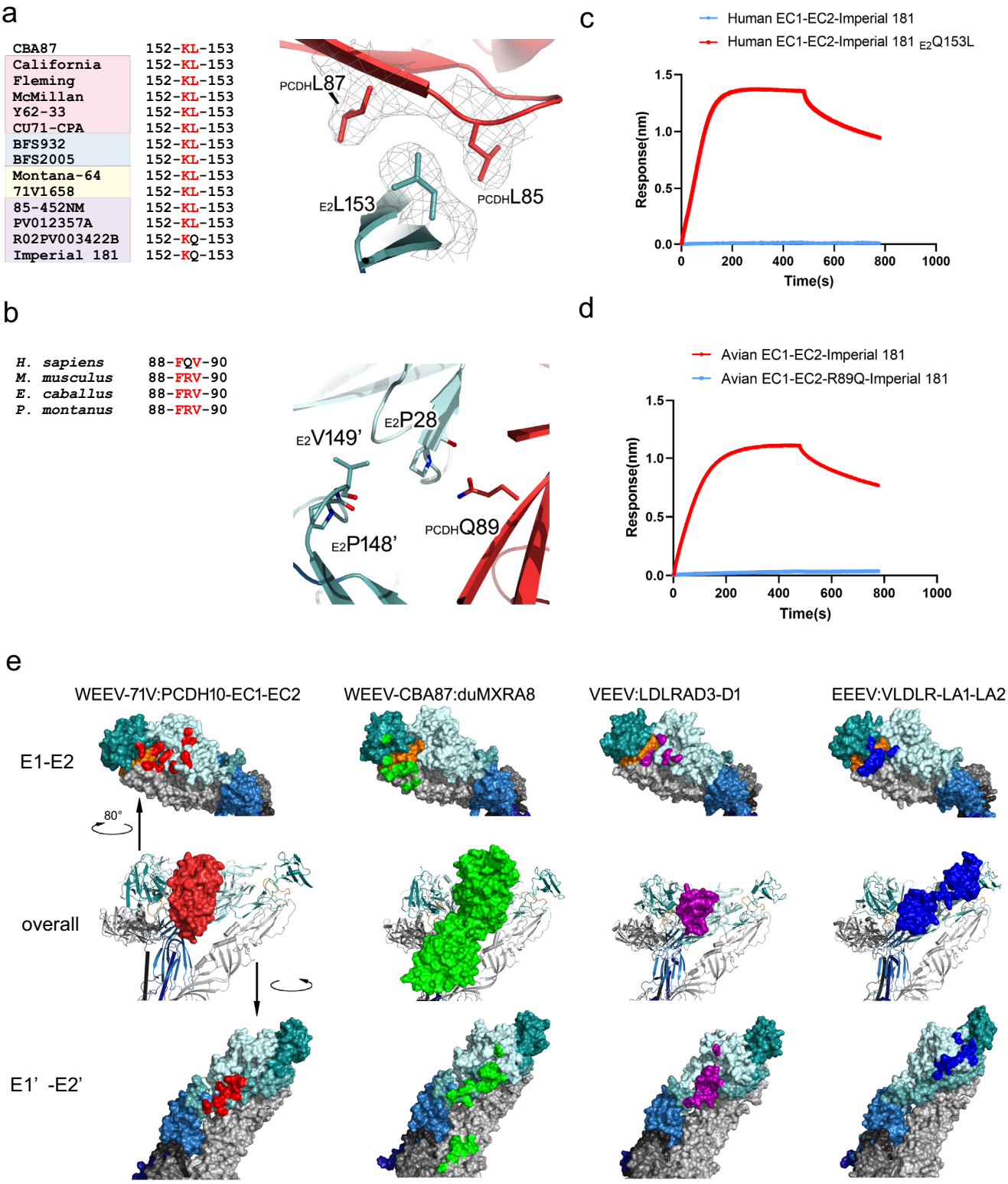

WEEV:PCDH10, VEEV:LDLARAD3, and EEEV:VLDLR complexes. The regions spanning residues 25–30, as well as residue 181 and adjacent residues, of E2 proteins in WEEV and their counterparts in other alphaviruses, are also involved in all three virus–receptor complexes. The region spanning residues 266-269 of E2 in WEEV and its counterpart in VEEV engage PCDH10/duMxra8 and LDLRAD3. The region covering residues 223–228 is a WEEV-specific region for interactions with both PCDH10 and the avian Mxra8. However, $_{E2}$D44, $_{E2}$G122, and $_{E2}$E125 of the E2 protein are uniquely involved in the binding of WEEV with PCDH10. Those structural information will be helpful in the discovery of potential wide-spectrum antibodies against alphaviruses.

Methods

Preparation of WEEV VLPs

The gene encoding the WEEV capsid and envelope proteins (strain 71V1658, GenBank NC_003908.1, Imperial 181, GenBank GQ287641.1) was codon-optimized and synthesized (GenScript, USA). The synthesized WEEV gene was cloned into the pCAGGS vector. HEK293F

Fig. 5 | Strain-specific residues analysis and comparative analysis of receptor binding of encephalitic alphaviruses. a Comparative analysis of position 153 of the E2 protein. Left panel, sequence alignment of position 152/153 of E2 proteins encoded by WEEV strains as labeled in the figure. Group A, B1, B2, and B3 are indicated by light pink, light blue, yellow, and light purple backgrounds. Red words denote the strictly conserved residues, whereas black words denote the non-conserved residues. Right panel, the interaction of $_{E2}$L153 with $_{PCDH}$L85/L87. Residues are shown as colored sticks covered by the cryo-EM densities as gray meshes. **b** Comparative analysis of position 89 of PCDH10. Left panel, sequence alignment of position 89 of PCDH10 from *Homo sapiens*, *Mus musculus*, *Equus caballus*, and *Passer montanus*. Red words denote the strictly conserved residues, whereas black words denote the non-conserved residues. Right panel, residue $_{PCDH}$Q89 and its environment WEEV residues $_{E2}$P28 and $_{E2}$P148′/V149′. Residues are shown as colored sticks. **c** BLI analyses of the binding of human PCDH10-EC1-EC2 to WEEV Imperial 181 VLPs and its mutant $_{E2}$Q153L. **d** BLI analyses of the binding of avian PCDH10-EC1-EC2 and its mutant R89Q to WEEV Imperial 181 VLPs (**e**) Comparative analysis of receptor binding of encephalitic alphaviruses. The structures of WEEV-71V:PCDH10-EC1-EC2 in this work, WEEV-CBA87:duMxra8 (PDB: 8DAN[23]), VEEV:LDLRAR3-D1 (PDB: 7N1H[29]) and EEEV:VLDLR-LA1-LA2 (PDB: 8UFC[30]) are aligned and shown in the same orientation. The color scheme is the same as that used in Fig. 2 and Supplementary Figs. 8 and 9. In the middle row, E2-E1 heterodimers are shown as cartoon diagrams, while the receptors are covered by red surfaces. In the top and bottom rows, E2-E1 (top) and E1′-E2′ (bottom) heterodimers are covered by molecular surfaces. The residues interacting with receptors are colored the same color as Supplementary Figs. 8 and 9.

cells were cultured in SMM 293 T-II medium (Sino Biological Inc., China) at 37 °C under 5% CO_2. The cells (500 mL culture) were seeded at 2×10^6 cells per mL and were subsequently transfected with a mixture of 1 mg of WEEV VLP plasmid and 3 mg polyethyleneimine (PEI; Polysciences, USA). After 96 h of transfection, the supernatant was collected by centrifugation at $1000 \times g$ for 15 min. The supernatant was centrifuged at $3000 \times g$ for 15 min and sterile-filtered using a 0.45 μM filter to remove the cell debris. The VLPs were subsequently pelleted through a 30% (w/v) sucrose cushion at 140,000 *g* for 3 h at 4 °C using a SW32 Ti rotor (Beckman Colter, USA). The resultant VLPs pellets were resuspended in the buffer (20 mM HEPES, 150 mM NaCl, pH 7.5), and were further purified by ultracentrifugation on a 20–60% (w/v) sucrose density gradient using a SW41 Ti rotor (Beckman Colter, USA) at 168,000 *g* for 12 h at 4 °C. The band of VLPs was carefully extracted using a syringe, buffer-exchanged into the buffer containing 20 mM HEPES, 150 mM NaCl, pH 7.5, and concentrated with an Amicon Ultra-4 300 kDa cut-off centrifugal concentrator (Millipore, USA). The particle integrity was checked using negative-stain electron microscopy, and VLPs were always used within seven days of purification.

Preparation of the recombinant PCDH10 protein and the mutations

The gene encoding human PCDH10 (GenBank NP_116586.1) EC1 (residues 19–122) and EC1-EC2 (residues 19–250) was codon-optimized and synthesized (SupraGene, China). Human PCDH10-EC1 and PCDH10-EC1-EC2 were cloned into the pCDNA3.4 vector with the native signal peptide sequence, followed by a human IgG1 Fc region. HEK293F cells (500 mL culture) were transfected with a mixture containing 1 mg of plasmids and 3 mg PEI at a cell density of 2.5×10^6 cells/mL. The supernatant was collected 72 h after transfection, centrifuged at $3000 \times g$ for 20 min, and sterile-filtered using a 0.45 μM filter to remove the cell debris and purified using protein A Sepharose 4B (GenScript, USA). After elution, the target protein was concentrated and purified by Superdex-200 size exclusion chromatography column (GE Healthcare, USA) in the buffer containing 20 mM HEPES, 150 mM NaCl, pH 7.5. Protein purity was assessed by SDS-PAGE analysis. The plasmids of PCDH10 mutants were constructed via site-directed mutagenesis, with each of the identified residues involved in binding with WEEV VLPs mutated separately.

Bio-layer interferometry (BLI) analysis

BLI analyses were performed by the ForteBio Octet Red system (ForteBio Inc., USA). The purified PCDH10-EC1-EC2-Fc or the mutated proteins (100 nM) were immobilized onto the AHC biosensors (Sartorius 18-5060) in 200 μl loading buffer (20 mM HEPES, 150 mM NaCl, 2 mM $CaCl_2$, 0.1% BSA, pH 7.5) for 100 s. Coated sensor tips were dipped into the kinetic buffer for a baseline measurement of 100 s, then dipped into wells containing the various concentrations of WEEV VLPs for 480 s. Subsequently, a buffer wash of 300 s was applied to allow the dissociation of molecules from the sensor. Data analysis was performed with the software Octet (v.6.4, ForteBio) using a standard 1:1 binding model. Two independent experiments were conducted for each sample.

Cell attachment and entry assay

The genome of the pseudotyped virus SINV-WEEV (71V-1658) was generated by the replacement of SINV C-E3-E2-6K-E1 with WEEV (71V-1658). In addition, an eGFP coding sequence was inserted downstream of the SINV subgenomic promoter. The genomic sequence of SINV-WEEV was synthesized (Sangon Biotech, China) and cloned into the pACYC177 vector. pACYC177 plasmids were linearized with SacI and in vitro transcribed using mMESSENGER mMACHINE T7 Kit (#AM1344, Invitrogen, USA) to generate SINV-WEEV RNAs. Viral RNAs were then transfected into BHK-21 cells with DMRIE-C (#10459014, Invitrogen, USA). Two days after transfection, the supernatant containing pseudotyped viruses was collected.

The Flag-tagged truncation and mutations of PCDH10 were constructed into the pMSCV vector. HEK293T cells were transduced with empty vector or the indicated PCDH10 expressing plasmids by retroviral-mediated gene transfer to establish the stable cell lines, followed by infection with SINV-WEEV (71-V1658) viruses. Cells were then collected with trypsin, and fixed with 4% paraformaldehyde diluted in PBS for 15 min and washed three times with PBS. Cells were processed on BD LSRFortessa, and analyzed using FlowJo software.

Cryo-EM sample preparation and data collection

The WEEV VLPs (71V-1658) were incubated with PCDH10-EC1-EC2-Fc for 2 hours on ice. Subsequently, the samples (4 μL) in the buffer (20 mM HEPES, 150 mM NaCl, pH 7.5) were applied onto a H_2/O_2 glow-discharged, 300-mesh Quantifoil R1.2/1.3 holey NiTi grids (Quantifoil, Micro Tools GmbH, Germany). The grid was then blotted for 5.0 s with a blot force of 0 at 8 °C and 100% humidity and plunge-frozen in liquid ethane using a Vitrobot[43] (Thermo Fisher Scientific, USA). Cryo-EM data for WEEV VLPs in complex with PCDH10-EC1-EC2-Fc were collected using a 300 kV Titan Krios electron microscope (Thermo Fisher Scientific, USA) equipped with a BM Falcon detector. The images were recorded at 75,000 × magnification with a super-resolution pixel size of 1.1 Å/pixel. The exposure time was set to 6.4 s, delivering a total accumulated dose of 50 electrons per Å^2. A total of 20,177 micrographs were automatically captured using the EPU software, with a defocus range from − 2.0 μm to − 1.0 μm. For WEEV VLPs alone, data were collected on the same 300 kV Titan Krios microscope, configured for EFTEM imaging, and equipped with a Quantum LS energy filter (10 eV slit width). The images were recorded at 105,000 × magnification with a super-resolution pixel size of 1.2 Å/pixel. The exposure time was set to 8.72 s with a total accumulated dose of 50 electrons per Å^2. A total of 3408 micrographs were automatically recorded using EPU and were collected with a defocus range from − 2.0 μm to − 1.0 μm. Statistics for data collection and refinement are provided in Supplementary Table 1.

Cryo-EM data processing

All dose-fractioned images were motion-corrected and dose-weighted by patch motion correction, and the contrast transfer function (CTF) of each micrograph was estimated by patch CTF estimation in cryoSPARC[44]. For WEEV VLP:PCDH10-EC1-EC2-Fc, a total of 17,711 micrographs were manually selected for further processing. First, 3000 micrographs were selected to perform blob picker and 2D classification. Particles from high-quality 2D classes were then used for training in Topaz. After Topaz extraction and 2 rounds of 2D classification, a total of 20,309 particles (236 pix, bin4) were selected for subsequent reconstruction. Bad classes representing supporting films, ice contaminations, or broken particles were excluded. The volume of WEEV-CBA87 VLP (EMD-27389) with low pass and 2 junk volumes generated from bad classes were used as references for heterogeneous refinement. 17,858 particles with clear WEEV VLP features were re-extracted with 472 pixels (bin2) and subjected to non-uniform refinement with I1 symmetry, yielding a reconstruction at the resolution of 5.90 Å. To further improve the resolution, the block-based reconstruction[45] was performed around the 5-fold axes region of the particles. 1,071,480 sub-particles were extracted (320 pix, bin1), defocus corrected and performed one round of 3D classification (with C1 symmetry) without alignment in relion3.1.2[46]. 99,107 particles from distinct vertex were selected for local refinement with C5 symmetry in cryoSPARC, resulting in a 3.37 Å reconstruction of the 5-fold axes region. Particles used for local refinement were symmetry expanded with C5 symmetry, and all the trimeric spikes from the 5-fold axes region were extracted (240 pixels, bin 1). After one round of local refinement with C3 symmetry, the resolution was improved to 3.14 Å. To further improve the receptor resolution, we performed symmetry expansion with C3 symmetry of trimeric spikes and performed focused classification without alignment in Relion3.1.2. The class with the clearest receptor signal (591,661 particles) was selected. After removing the duplicates, 378,489 trimeric spikes were used for further refinement. All these trimeric spikes were performed by local refinement (C3 symmetry), reference-based motion correction, and CTF refinement in cryoSPARC, yielding a final resolution at 2.99 Å. For the data set of WEEV VLPs alone, 3106 micrographs were manually selected for further processing. Following similar particle sorting and block-based reconstruction strategies, the final resolutions of WEEV VLPs and the trimeric spikes are achieved at 4.50 Å and 2.53 Å, respectively. Automatic local sharpening in EMReady[47] was performed to improve the densities. The local resolutions were estimated in cryoSPARC. The workflow is shown in Supplementary Fig. 2.

Model building and refinement

To build the structures of WEEV VLP and its complex with PCDH10-EC1-EC2-Fc, the coordinates of E1 and E2 proteins of WEEV strain CBA87 VLP (PDB: 8DEE[23]), as well as EC1 domain of human PCDH10 (PDB: 6VG4[33]) were individually placed and fitted by rigid-body refinement into the cryo-EM maps in UCSF Chimera[48]. The models were rebuilt using Coot[49] with the guidance of the cryo-EM maps and were refined with real-space refinement using Phenix[50]. The data validation statistics are shown in Supplementary Table 1. Structural figures were generated with Pymol[51], UCSF Chimera, and ChimeraX[52].

Reporting summary

Further information on research design is available in the Nature Portfolio Reporting Summary linked to this article.

Data availability

The cryo-EM density maps and the structures generated in this study were deposited into the Electron Microscopy Data Bank (EMDB) and Protein Data Bank (PDB) with the accession numbers EMDB (EMD-62791) and PDB (9L3V) for WEEV strain 71V1658 VLPs alone, EMDB (EMD-62802) and PDB (9L41) for the complex with PCDH10-EC1-EC2-Fc. The source data underlying Figs. 3, – 5, and Supplementary Fig. 1 are provided as a Source Data file. Specific data *P*-values are also included within the Source Data File. Source data are provided in this paper.

References

1. Chen, W. et al. Arthritogenic alphaviruses: new insights into arthritis and bone pathology. *Trends Microbiol.* **23**, 35–43 (2015).
2. Powers, A. M. et al. Evolutionary relationships and systematics of the alphaviruses. *J. Virol.* **75**, 10118–10131 (2001).
3. Ronca, S. E., Dineley, K. T. & Paessler, S. Neurological sequelae resulting from encephalitic Alphavirus infection. *Front. Microbiol.* **7**, 959 (2016).
4. Mejía, C. R. & López-Vélez, R. Tropical arthritogenic alphaviruses. *Reumatol. Clin.* **14**, 97–105 (2018).
5. Bergren, N. A. et al. Submergence" of Western equine encephalitis virus: Evidence of positive selection argues against genetic drift and fitness reductions. *PLoS Pathog.* **16**, e1008102 (2020).
6. Reisen, W. K. & Wheeler, S. S. Surveys for antibodies against mosquitoborne encephalitis viruses in California birds, 1996-2013. *Vector Borne Zoonotic Dis.***16**, 264–282 (2016).
7. Reed, D. S. et al. Aerosol exposure to western equine encephalitis virus causes fever and encephalitis in cynomolgus macaques. *J. Infect. Dis.* **192**, 1173–1182 (2005).
8. Carey, B. D., Bakovic, A., Callahan, V., Narayanan, A. & Kehn-Hall, K. New World alphavirus protein interactomes from a therapeutic perspective. *Antivir. Res.* **163**, 125–139 (2019).
9. Zanotto, P. M. A. & Leite, L. C. C. The challenges imposed by Dengue, Zika, and Chikungunya to Brazil. *Front. Immunol.* **9**, 1964 (2018).
10. Strauss, J. H. & Strauss, E. G. The alphaviruses: gene expression, replication, and evolution. *Microbiol. Rev.* **58**, 491–562 (1994).
11. Lescar, J. et al. The Fusion glycoprotein shell of Semliki Forest virus: an icosahedral assembly primed for fusogenic activation at endosomal pH. *Cell* **105**, 137–148 (2001).
12. Smith, T. J. et al. Putative receptor binding sites on alphaviruses as visualized by cryoelectron microscopy. *Proc. Natl. Acad. Sci. USA* **92**, 10648–10652 (1995).
13. Zhang, W., Heil, M., Kuhn, R. J. & Baker, T. S. Heparin binding sites on Ross River virus revealed by electron cryo-microscopy. *Virology* **332**, 511–518 (2005).
14. DeTulleo, L. & Kirchhausen, T. The clathrin endocytic pathway in viral infection. *EMBO J.* **17**, 4585–4593 (1998).
15. Lee, R. C. et al. Mosquito cellular factors and functions in mediating the infectious entry of chikungunya virus. *PLoS Negl. Trop. Dis.* **7**, e2050 (2013).
16. Li, L., Jose, J., Xiang, Y., Kuhn, R. J. & Rossmann, M. G. Structural changes of envelope proteins during alphavirus fusion. *Nature* **468**, 705–708 (2010).
17. Roussel, A. et al. Structure and interactions at the viral surface of the envelope protein E1 of Semliki Forest virus. *Structure* **14**, 75–86 (2006).
18. Voss, J. E. et al. Glycoprotein organization of Chikungunya virus particles revealed by X-ray crystallography. *Nature* **468**, 709–712 (2010).
19. Kostyuchenko, V. A. et al. The structure of barmah forest virus as revealed by cryo-electron microscopy at a 6-angstrom resolution has detailed transmembrane protein architecture and interactions. *J. Virol.* **85**, 9327–9333 (2011).
20. Pletnev, S. V. et al. Locations of carbohydrate sites on alphavirus glycoproteins show that E1 forms an icosahedral scaffold. *Cell* **105**, 127–136 (2001).
21. Zhang, R. et al. 4.4 Å cryo-EM structure of an enveloped alphavirus Venezuelan equine encephalitis virus. *EMBO J.* **30**, 3854–3863 (2011).
22. Zhang, R. et al. Mxra8 is a receptor for multiple arthritogenic alphaviruses. *Nature* **557**, 570–574 (2018).

23. Zimmerman, O. et al. Vertebrate-class-specific binding modes of the alphavirus receptor MXRA8. *Cell* **186**, 4818–4833 (2023).
24. Clark, L. E. et al. VLDLR and ApoER2 are receptors for multiple alphaviruses. *Nature* **602**, 475–480 (2022).
25. Ma, H. et al. LDLRAD3 is a receptor for Venezuelan equine encephalitis virus. *Nature* **588**, 308–314 (2020).
26. Basore, K. et al. Cryo-EM Structure of Chikungunya virus in complex with the Mxra8 receptor. *Cell* **177**, 1725–1737.e1716 (2019).
27. Song, H. et al. Molecular basis of Arthritogenic Alphavirus receptor MXRA8 binding to Chikungunya virus envelope protein. *Cell* **177**, 1714–1724 (2019).
28. Ma, B., Huang, C., Ma, J., Xiang, Y. & Zhang, X. Structure of Venezuelan equine encephalitis virus with its receptor LDLRAD3. *Nature* **598**, 677–681 (2021).
29. Basore, K. et al. Structure of Venezuelan equine encephalitis virus in complex with the LDLRAD3 receptor. *Nature* **598**, 672–676 (2021).
30. Adams, L. J. et al. Structural and functional basis of VLDLR usage by Eastern equine encephalitis virus. *Cell* **187**, 360–374 (2024).
31. Li, W. et al. Shifts in receptors during submergence of an encephalitic arbovirus. *Nature*, https://doi.org/10.1038/s41586-024-07740-2 (2024).
32. Yang, Y. et al. PCDH10 is a neuronal receptor for western equine encephalitis virus. *Cell Res.* **34**, 802–805 (2024).
33. Harrison, O. J. et al. Family-wide structural and biophysical analysis of binding interactions among non-clustered δ-Protocadherins. *Cell Rep.* **30**, 2655–2671 (2020).
34. Hoshina, N. et al. ASD/OCD-Linked protocadherin-10 regulates synapse, but not Axon, development in the Amygdala and contributes to fear- and anxiety-related behaviors. *J. Neurosci.* **42**, 4250–4266 (2022).
35. Tsai, N. P. et al. Multiple autism-linked genes mediate synapse elimination via proteasomal degradation of a synaptic scaffold PSD-95. *Cell* **151**, 1581–1594 (2012).
36. Nagata, L. P. et al. Infectivity variation and genetic diversity among strains of Western equine encephalitis virus. *J. Gen. Virol.* **87**, 2353–2361 (2006).
37. Logue, C. H. et al. Virulence variation among isolates of western equine encephalitis virus in an outbred mouse model. *J. Gen. Virol.* **90**, 1848–1858 (2009).
38. Cao, D., Ma, B., Cao, Z., Zhang, X. & Xiang, Y. Structure of Semliki Forest virus in complex with its receptor VLDLR. *Cell* **186**, 2208–2218 (2023).
39. Park, Y.-J. et al. Molecular basis of convergent evolution of ACE2 receptor utilization among HKU5 coronaviruses. *Cell* **188**, 1711–1728 (2025).
40. Chen, J. et al. Bat-infecting merbecovirus HKU5-CoV lineage 2 can use human ACE2 as a cell entry receptor. *Cell* **188**, 1729–1742 (2025).
41. Ma, C.-B. et al. Multiple independent acquisitions of ACE2 usage in MERS-related coronaviruses. *Cell* **188**, 1693–1710 (2025).
42. Song, H. et al. Receptor binding, structure, and tissue tropism of cattle-infecting H5N1 avian influenza virus hemagglutinin. *Cell* **188**, 919–929 (2025).
43. Kang, J. S., Zhou, X., Liu, Y.-T., Wang, K. & Zhou, Z. H. Theoretical framework and experimental solution for the air–water interface adsorption problem in cryoEM. *Biophys. Rep.* **9**, 215–229 (2023).
44. Punjani, A., Rubinstein, J. L., Fleet, D. J. & Brubaker, M. A. cryoSPARC: algorithms for rapid unsupervised cryo-EM structure determination. *Nat. Methods* **14**, 290–296 (2017).
45. Zhu, D. et al. Pushing the resolution limit by correcting the Ewald sphere effect in single-particle Cryo-EM reconstructions. *Nat. Commun.* **9**, 1552 (2018).
46. Scheres, S. H. RELION: implementation of a Bayesian approach to cryo-EM structure determination. *J. Struct. Biol.* **180**, 519–530 (2012).
47. He, J., Li, T. & Huang, S. Y. Improvement of cryo-EM maps by simultaneous local and non-local deep learning. *Nat. Commun.* **14**, 3217 (2023).
48. Goddard, T. D. et al. UCSF ChimeraX: Meeting modern challenges in visualization and analysis. *Protein Sci.* **27**, 14–25 (2018).
49. Emsley, P., Lohkamp, B., Scott, W. G. & Cowtan, K. Features and development of Coot. *Acta Crystallogr. D. Biol. Crystallogr.* **66**, 486–501 (2010).
50. Afonine, P. V. et al. Real-space refinement in PHENIX for cryo-EM and crystallography. *Acta Crystallogr. D. Struct. Biol.* **74**, 531–544 (2018).
51. Schrodinger, L. L. C. *The PyMOL Molecular Graphics System, Version 1.8* (2015).
52. Pettersen, E. F. et al. UCSF ChimeraX: Structure visualization for researchers, educators, and developers. *Protein Sci.* **30**, 70–82 (2021).

Acknowledgements

This work was supported by the National Natural Science Foundation of China (32188101 and U20A20135) to Z.L., the R&D Program of Guangzhou Laboratory (SRPG22-003, GZNL2023A01008 and GZNL2024A01014) to R.Z., the National Key R&D Program of China (2023YFC2306100 and 2023YFC2305900) to Y.W. We thank the Electron Microscopy Facilities of Zhengzhou University and Guangzhou Laboratory for the cryo-EM data collection.

Author contributions

Z.R., Y.W., and Z.L. conceived the project and designed the experiments. S.L., Z.X., J.H., X.L., and D.L. prepared the WEEV VLPs and receptor proteins. Y.Y., S.L., L.Z., X.L., and C.H. performed the BLI analysis and cell-based assays. S.L. prepared the cryo-EM samples and collected the cryo-EM data. Y.L. and S.L. processed cryo-EM data and built the atomic model. Z.R., Y.W., and Z.L. analyzed the data. Z.L., Y.W., Z.R., and S.L. wrote the manuscript. All authors discussed the experiments, read, and approved the manuscript.

Competing interests

The authors declare no competing interests.

Additional information

Supplementary information The online version contains supplementary material available at https://doi.org/10.1038/s41467-025-61659-4.

Correspondence and requests for materials should be addressed to Zihe Rao, Yanyi Wang or Zhiyong Lou.

Peer review information *Nature Communications* thanks Andrew Ward, who co-reviewed with Kylie Konrath, for their contribution to the peer review of this work. A peer review file is available.